Complex Systems **8** (1994) 385–405

Self-Organization and Scaling in a Lattice Predator-Prey Model

B. R. Sutherland
D.A.M.T.P., University of Cambridge,
Cambridge, England CB3 9EW

A. E. Jacobs
Department of Physics,
University of Toronto,
Toronto, Canada M5S 1A7

Abstract. We propose that self-organization may provide a mechanism by which power-law cluster distributions of mobile prey (i.e., fish, phytoplankton) may develop; in contrast, such distributions have often been attributed to scaling of the background environment. Evidence supporting our proposal is provided by examining the dynamics of a cellular automaton-like model of a predator-prey system. The model, which is discrete in space and time, is robust and evolves to a state with oscillatory, phase-shifted populations for a large range of parameter values, namely the predator and prey breeding times and the predator starvation time. The distribution function $\overline{D}(s)$ of the prey cluster sizes s has roughly power-law form, $\overline{D}(s) \propto s^{-\alpha}$, over a range of moderately large sizes but is cut off at large s. The exponent $\alpha \simeq 1.35 \pm 0.10$ depends only weakly on the parameters of the model.

1. Introduction

The study of predator-prey interactions includes a diverse class of systems in which, for example, fish eat plankton, wolves attack deer, or a fire engulfs a forest. In such systems the average number of predators and prey have been observed to oscillate about some average "population" although the amplitude and period of the oscillations may vary greatly in time. Typically, because the number of predators tends to increase when there is an abundance of prey and the number tends to decrease when prey are scarce, the predator population cycle lags that of the prey.

Mathematical models of these interactions inherently involve nonlinear dynamics. For example, the classical description of a predator-prey system

is given by the Lotka-Volterra equations (e.g., Hedrick [8]) which constitute a coupled, nonlinear set of differential equations

$$\begin{aligned} \frac{d}{dt}P_f &= \alpha_f P_f(1 - \frac{\beta_1}{\alpha_f}P_s), \\ \frac{d}{dt}P_s &= -\alpha_s P_s(1 - \frac{\beta_2}{\alpha_s}P_f), \end{aligned} \tag{1}$$

in which the prey and predator populations are P_f and P_s, respectively, α_f is the prey breeding rate in the absence of predators, α_s is the predator death rate in the absence of prey, and β_1 and β_2 are interaction coefficients. If the prey and predator populations are assumed to be homogeneously distributed, then β_1 represents the probability per unit time that a predator encounters and eats a prey and β_2 represents the probability that a predator encounters and devours enough prey per unit time to ensure its survival. With empirically determined parameters, equation (1) adequately reproduces the basic dynamics of a predator-prey system in that both populations oscillate about mean values and the predator population lags that of the prey. In reality, however, the prey and predator populations are inhomogeneously distributed since, as is well known, prey often gather in clusters (schools, herds, gaggles, etc.), which provide some protection from predation. Attempts have been made to extend the Lotka-Volterra equations to include the effects of spatial and temporal variations of an ecological system (e.g., by incorporating diffusive effects [13]). However, these models do not describe the process of clustering, nor do such techniques seem capable of predicting the distribution of cluster sizes in an ecosystem. Indeed, Hastings [6] has pointed out that two of the most frequently employed models, diffusion-based models and patch models, appear to be applicable over only a limited range of spatial and temporal scales. It now appears that an understanding of the detailed spatial distributions for both species is necessary in order to describe appropriately the dynamics of such systems. For example, in their study of predation of Atlantic cod upon capelin in the Western Atlantic Ocean, Rose and Leggett [16] showed that the spatial correlation between the densities of the predators and prey was dependent on cluster size as well as environmental factors. Power-law spatial distributions of species have been demonstrated to appear in observations of plankton communities by Haury *et al.* [7] and in Holling's survey of a wide range of ecosystems, including birds and mammals in the boreal forest and boreal prairie [9]. To explain these structures, environmental factors such as the fractal distribution of energy resources and landscapes have often been called upon, but we show here that an alternative mechanism, that of self-organization, may also give rise to a power-law distribution of clusters.

The capacity for systems with intrinsic nonlinear feedback mechanisms to evolve to an organized state characterized by a nonscale selective geometry has been noted for many diverse natural phenomena (e.g., Mandelbrot [14]). In particular, Kauffman [12] has noted that self-organization is inherent to many biological and ecological systems. Significant progress has been made recently toward understanding the essential dynamics that determine the

power-law scaling behavior of self-organizing systems through the development and analysis of cellular automata (CA) and automaton-like models such as the one that we employ here. CA have proven to be particularly useful for the study of self-organizing systems because with only a limited set of basic instructions they are capable of producing patterns similar to many of the complex spatial structures and temporal behaviors that are observed in nature. For example, CA have been developed to study the size and frequency distribution of avalanches and earthquakes [2, 10, 11], the spatial development of a reactive chemical system [4], and the structure of an Ising spin system [15]. Although such models are often too crude to simulate accurately the dynamics of the real driven-dissipative system, they provide an appealing description for self-organization unattainable through standard algebraic techniques.

A variety of CA and CA-like models have been adapted to simulate various processes in ecological systems. Some, such as the so-called "Game of Life" [1], which models the interactions of a single species in competition with itself, lack robustness and randomness (after the setting of initial conditions) and so have questionable applicability to real ecological systems. The "Forest-Fire Model" [3] may be interpreted as a predator-prey model in which the prey ("trees") are attacked by a predator ("fire"). Computer simulations with many adjustable parameters have also been developed to simulate the dynamics of more complex ecosystems. But these assume the existence of spatial scaling of resources in the environment that influence the development of spatial scaling among elements of the ecosystem a priori. Conversely, we study a modified version of the CA-like model "Wa-Tor" due to Dewdney [5] that includes only those dynamics which are necessary for realistic evolution of a predator-prey system. We show that the simulations are robust in the sense that for a wide range of parameters they evolve in a continuous state of change but that they nonetheless exhibit scaling behavior. That is, the scaling behavior arises naturally in the model without ad hoc assumptions. Nonetheless, the long time behavior is, on average, in accordance qualitatively with the predictions of the Lotka-Volterra equations.

In our model, predators and prey (labeled "sharks" and "fish," respectively, by Dewdney) move on a square doubly periodic grid of linear size N such that each grid point is occupied by at most one individual. The model is similar to CA in the sense that prey and predators move, if possible, to one of the four neighboring sites and so predator-prey interactions are determined by local rules. The model is not deterministic, however, since the direction of motion is randomly selected. Furthermore, breeding and starvation, which occur for prey and predators at preset times according to the model parameters, are determined not by the instantaneous state of the system but rather by the values of internal clocks carried by each individual. The nonlocal temporal rules of the model are a departure from the usual class of CA but these are necessary to capture the dynamics of a predator-prey system. The rules of the model are discussed in detail in section 2.

In section 3 it is shown that, for a broad range of parameters, simulations of Wa-Tor evolve in a nontrivial manner for long times and exhibit the basic properties of predator-prey systems. We show also that the distribution $D(s)$ of prey cluster sizes s has power-law behavior at small sizes ($1 < s < 20$), and more importantly, also at large sizes ($100 < s < 500$). Both exponents (α' for small s and α for large s) depend only weakly on the model parameters. For very large clusters ($s > s_c$), the distribution of cluster sizes decreases approximately exponentially and so the distribution function is subcritical. The value s_c is implicitly determined by the dynamics of the interacting species; provided that the domain size is sufficiently large, finite-size effects are negligible. The relatively large value of s_c (typically s_c is of the order 1000 for simulations performed with the model parameters discussed herein) suggests that the model is near the edge of chaos [12]. Finally, we show that large prey clusters are compact for a wide range of parameters.

2. Description of the model

Our model applies only the most basic rules of an ecological system: both species move, both reproduce with a time lag, prey are devoured by nearby predators, and a predator dies when it has not eaten for a sufficiently long time. Each individual carries an internal clock specifying its age A defined to be the number of time steps elapsed since the individual was born. Each predator also carries a second clock (the "hunger time") that specifies the number of time steps elapsed since the predator last ate a prey (or since it was born). Both species breed by parthenogenesis with probability

$$P(A;b) = \frac{1}{2}\left[1 + \mathrm{erf}\left(\frac{A-b}{\sigma}\right)\right] \tag{2}$$

provided that the parent can move to at least one of its four nearest-neighbor (NN) sites. In equation (2), the parameter b is fb for prey and sb for predators. Here $\mathrm{erf}(x)$ is the error function defined by $\mathrm{erf}(x) = 2/\sqrt{\pi}\int_0^x \exp(-t^2)dt$, a function that increases smoothly from -1 to 1 over an interval of length ≈ 1. In Dewdney's original model [5], $\sigma = 0^+$ so that breeding occurs at precisely the time when $A = b$. In this case, however, the predator ages tend to synchronize into cycles of period sb since there is no inherent process in the rules of Wa-Tor to randomize the age of a single parent. We use $\sigma = 0.5$ in order to prevent this unphysical synchronization while maintaining a quasi-regular breeding cycle. During each birth event, the offspring are placed at the original site and at one of the NN sites. The ages for the offspring of predators and prey and the hunger clocks for the offspring of predators are set to zero.

The simulation is initialized at time $t = 0$ by randomly distributing nf prey and ns predators on an N by N square grid. For nontrivial final states, the initial predator and prey numbers must be sufficiently large; typically, nf and ns are set so that the initial densities of prey and predators are 0.20 and 0.05, respectively (i.e., $nf = 0.2N^2$ and $ns = 0.05N^2$). Each time step

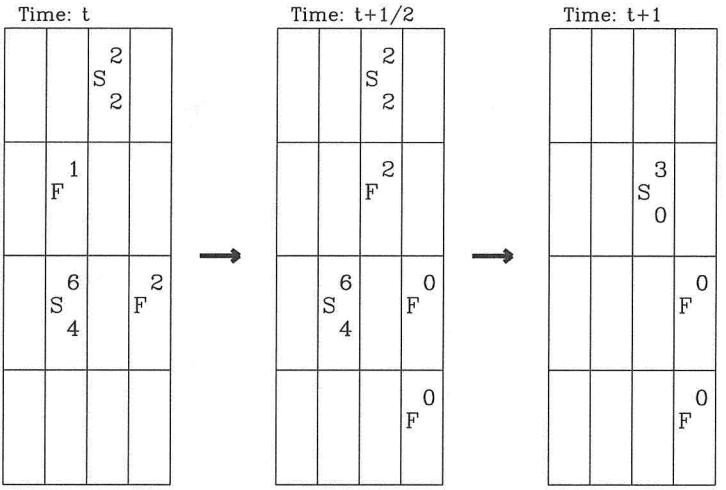

Figure 1: Example of Wa-Tor rules for a simulation with parameters $fb = 2$, $sb = 8$, and $ss = 4$. A position on the grid can be occupied either by a predator or a prey (designated by S or F, respectively). The superscripts to each species type indicates the age and the subscript to S indicates the time since the predator last ate a prey. When prey or predators breed, they do so by parthenogenesis and the age of both offspring is zero.

begins with a sweep over the prey. Each prey either gives birth in the manner described above or does not give birth; in the latter case it randomly moves to an NN site, provided that the site is vacant. The time step is completed by a sweep over the predators. Those that have not eaten after ss time steps (the starvation time) are removed from the grid. Then, if permissible, births occur. Finally, predators that do not give birth move to any NN site occupied by a prey (and devour it); otherwise they move to any NN site not occupied by a predator. After both species have moved, one time step is said to have elapsed. An example of the motion of predators and prey in one time step is shown in Figure 1.

In our implementation of the rules, the data relevant to each prey and predator are stored in a linked list. This approach, unlike sequential scanning, ensures that there is no inherent directional bias to the motion. For both species, each element of the list contains the individual's position on the grid and its age. For predators, the list also contains the hunger time.

The rules of Wa-Tor can be extended in many ways, including the following modifications which we have examined.

1. Competition among prey is included, whereby prey are said to starve if they remain within a large cluster for a certain number fs time steps.

2. Simulations have been performed so that when individuals give birth the age of only one offspring is set to zero.

3. The sensitivity of the dynamics to the restrictions of the underlying grid have been examined by performing simulations in which the prey and predators may move to one of eight nearest neighbors (motion on the so-called "Moore" grid) and also by allowing both species to move on a grid in three spatial dimensions.

Simulations performed with these modified rules demonstrate qualitatively similar results: the simulations are robust, the predator and prey populations oscillate with a phase lag, and the prey cluster size distribution obeys a power law over a large range of cluster sizes. However, since the appeal of the model lies largely in the simplicity of its rules, which are nonetheless capable of reproducing the fundamental and yet complex dynamics of observed predator-prey systems, a detailed analysis has been performed only for the original rules described above.

3. Results and analysis

Simulations have been performed for a large range of parameters fb, sb, and ss on an N by N square grid. The model is robust: for many values of fb,sb,ss, and N, and for a wide range of initial conditions, the system evolves nontrivially for long times. To demonstrate this detailed tests for robustness have been made for simulations on a grid with $N = 50$ and initial prey and predator population densities of 0.20 and 0.05, respectively. Trivial states are reached when one or both species become extinct but, for many sets of parameters fb, sb, and ss, nontrivial final states have been observed after 5000 time steps. In these tests, the prey and predator populations typically exhibit oscillations with a period of about 50 time steps and nontrivial simulations evolve through approximately 100 periods with no apparent indication that either species may eventually become extinct. In particular, nontrivial final states have been observed for $fb = 1$, $sb = 10$, with ss ranging from 1 to 8, for $fb = 1$, $ss = 1$, with sb ranging from 1 to at least 16, and for $sb = 10$, $ss = 5$, with fb ranging from 1 to 13. A trivial final state is reached if the predator starvation time ss exceeds the predator breeding time since, in this case, there is no factor limiting the growth of the predator population save the domain size. A trivial final state is also reached if the breeding time of the prey is moderately larger than that of the predators. For parameters near values for which a trivial state is reached, the final state of the simulation is sensitive to the initial population densities, positions, and ages of prey and predators. For intermediate parameter values, the simulation is sensitive to the initial state for domain sizes with $N < 40$. Otherwise, the same quantitative observations are made for different random initial positions and population densities.

For most of the investigations that follow a detailed analysis has been performed for the parameter set $fb = 4$, $sb = 8$, and $ss = 4$. This choice

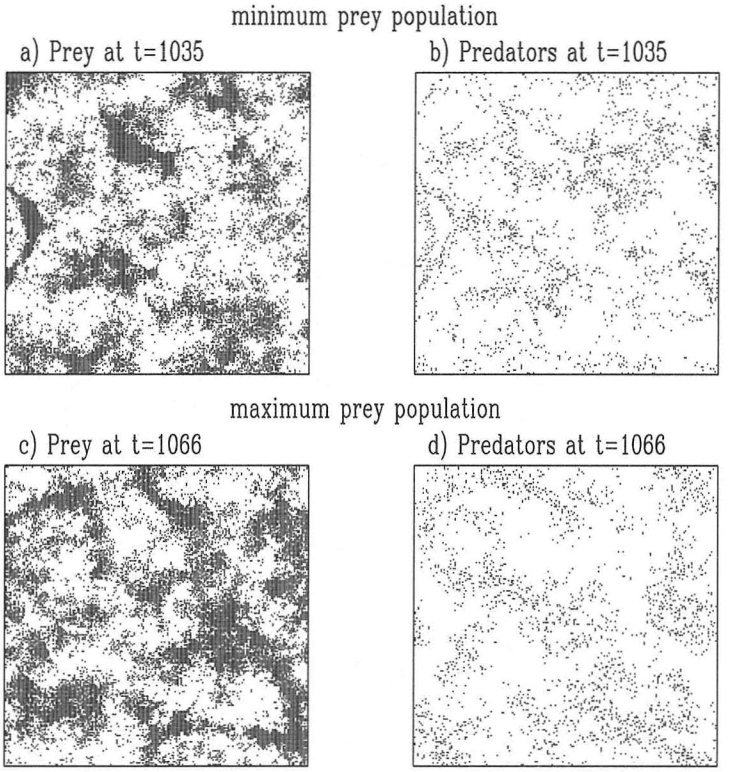

Figure 2: Predator and prey positions at times $t = 1035$, and $t = 1066$ for a simulation with the standard parameter set ($fb = 4$, $sb = 8$, and $ss = 4$) on a grid with $N = 200$. At time $t = 1035$ the prey population is at a local minimum and at $t = 1066$ the population is at a local maximum.

of parameters is referred to hereafter, though somewhat arbitrarily, as the "standard" set. Simulations run with these parameters and with other parameter sets consisting of values close to them are relatively insensitive to the initial conditions on grids with $N > 50$, and hence useful comparisons can be made of the average populations and scaling exponents for a range of parameters around the standard set. Furthermore, the time scales implicitly determined by the standard set are small so that the data may be collected for many population cycles in a small number of time steps. The time scale is large enough, however, that both the predators and prey usually move more than one site from their birth place before breeding.

In Figure 2 the positions of predators and prey are shown for simulations run with the standard parameter set on a grid with $N = 200$ at times $t = 1035$ and 1066 for which the prey population cycle is at a local minimum and a

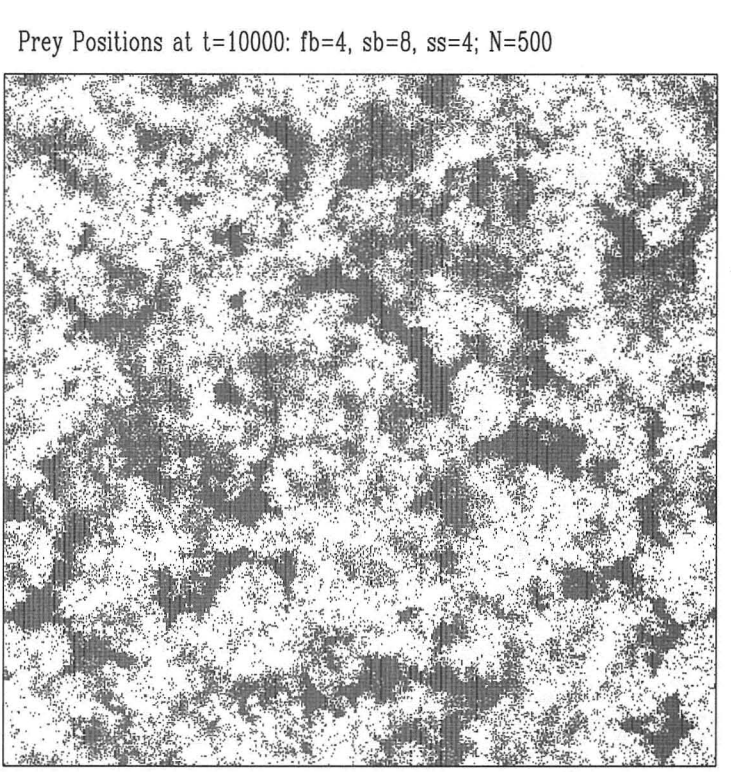

Figure 3: Prey positions on a grid with $N = 500$ at time $t = 10000$. The simulation is performed with the standard parameter set. The diagram demonstrates that the size of the largest clusters is not limited by the domain size.

local maximum, respectively. The self-organization of prey into clusters is evident from these diagrams. The clustering occurs due to both the birth rules and the merging of smaller clusters. The predators are most densely located near the perimeters of the larger clusters. As shown below, the distribution of the prey cluster size has scaling behavior over two ranges. The scaling behavior of large clusters is limited, however, by a self-induced cut-off size s_c which is not due to the finite domain size. Qualitatively, this is evident in Figure 3 which shows the prey distribution on a large grid with $N = 500$ for a simulation run with the standard parameter set. The figure, which is taken from the simulation at time $t = 10000$, clearly demonstrates the complex and dynamic arrangement of the prey.

The prey organize into clusters with similar scaling behavior for other parameters as demonstrated quantitatively in Figure 4 which shows the prey positions for simulations on a grid with $N = 200$ at times after $t = 1000$

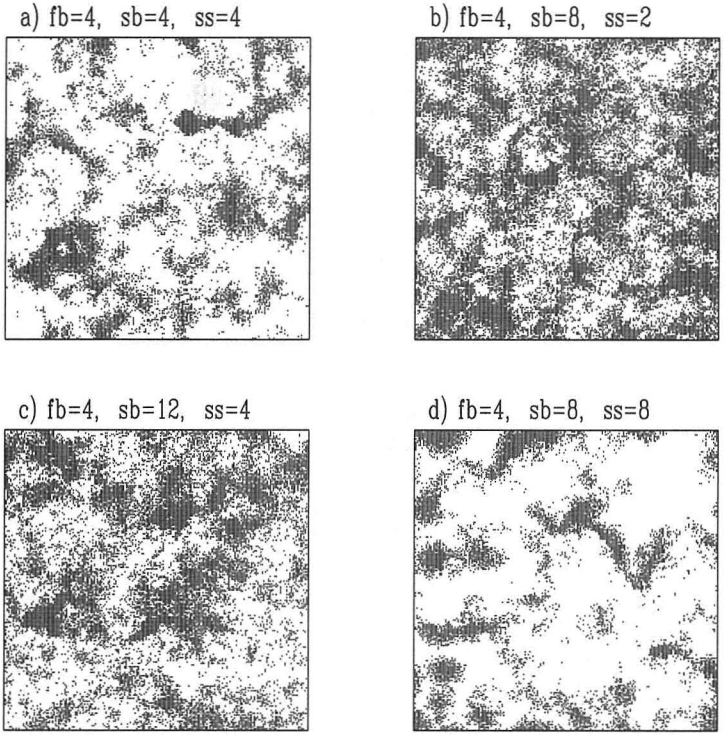

Figure 4: Prey positions on a grid with $N = 200$ for simulations with parameters a) $fb = 4$, $sb = 4$, $ss = 4$, b) $fb = 4$, $sb = 8$, $ss = 2$, c) $fb = 4$, $sb = 12$, $ss = 4$, and d) $fb = 4$, $sb = 8$, $ss = 8$. The times for each diagram shown are chosen to be the shortest time after $t = 1000$ for which the prey population is approximately equal to the population average and is increasing.

when the prey population is near the average population and is increasing. The two left-most diagrams show the effect of changing the predator breeding time from the standard value, $sb = 8$, to $sb = 4$ (diagram a) and $sb = 12$ (diagram c). The two right-most diagrams show the effect of changing the predator starvation time from the standard value, $ss = 4$, to $ss = 2$ (diagram b) and $ss = 8$ (diagram d). It is apparent from these diagrams that the prey clusters tend to be larger when the breeding time of the predators is large compared to the starvation time. Because the population densities of prey are large in such cases (e.g., Figures 4b and 4c) a grid with $N = 200$ may not be sufficiently large to avoid finite-size effects. Most of the detailed analyses of the predator and prey populations and of the prey clusters are presented for simulations on a grid with $N = 300$ which has been found to be adequately large.

Parameters		$\overline{P_f}$	$\overline{P_s}$	A_0	α'	α
$fb = 4$	$N = 50$	0.372	0.058	7.6	2.32	1.32
$sb = 8$	$N = 100$	0.366	0.059	7.4	2.33	1.31
$ss = 4$	$N = 200$	0.359	0.059	7.3	2.34	1.31
	$N = 300$	0.361	0.059	7.3	2.34	1.29
	$N = 400$	0.360	0.059	7.3	2.34	1.31
$N = 300$	$fb = 2$	0.354	0.083	5.2	2.26	1.31
$sb = 8$	$fb = 4$	0.361	0.059	7.3	2.34	1.29
$ss = 4$	$fb = 6$	0.362	0.047	9.2	2.38	1.28
	$fb = 8$	0.359	0.039	11.0	2.39	1.29
$N = 300$	$sb = 4$	0.243	0.063	6.7	2.39	1.43
$fb = 4$	$sb = 6$	0.314	0.061	7.0	2.38	1.29
$ss = 4$	$sb = 8$	0.361	0.059	7.3	2.34	1.29
	$sb = 10$	0.387	0.059	7.5	2.30	1.31
	$sb = 12$	0.406	0.058	7.5	2.26	1.33
	$sb = 14$	0.422	0.058	7.6	2.23	1.37
	$sb = 16$	0.433	0.058	7.6	2.20	1.39
$N = 300$	$ss = 2$	0.502	0.057	8.1	2.17	1.31
$fb = 4$	$ss = 4$	0.361	0.059	7.3	2.34	1.29
$sb = 8$	$ss = 6$	0.270	0.061	6.7	2.42	1.30
	$ss = 8$	0.204	0.063	6.7	2.43	1.37
$N = 300$	$fb = 20$	0.224	0.023	30.0	2.56	1.35
$sb = 40$	$ss = 20$					

Table 1: Average prey and predator population densities, the half-life A_0 of old prey ($20 \leq A \leq 100$), and prey cluster scaling exponents α' and α for small ($1 \leq s \leq 20$) and large ($100 \leq s \leq 500$) clusters, respectively. The linear grid size is N and the parameters fb, sb, and ss are defined in the text. The average population densities and exponents are calculated from simulations for times between 1000 and 10000 in each case. The results given in the table are quoted to the accuracy of the associated errors.

Table 1 summarizes most of the results to be presented in the following sections by listing values of the relevant quantitative features of the model run under different parameters. The table lists values of P_f and P_s, the average prey and predator populations; A_0, a measure of the life expectancy of prey within large clusters; and α' and α, which measure the scaling behavior of clusters of prey at small and large cluster sizes. Each of these quantities will be described in detail in the following sections and an interpretation of the results will be given.

3.1 Population analysis

If the initial population densities of the predators and prey are sufficiently large, the populations of both species rapidly settle into oscillations with

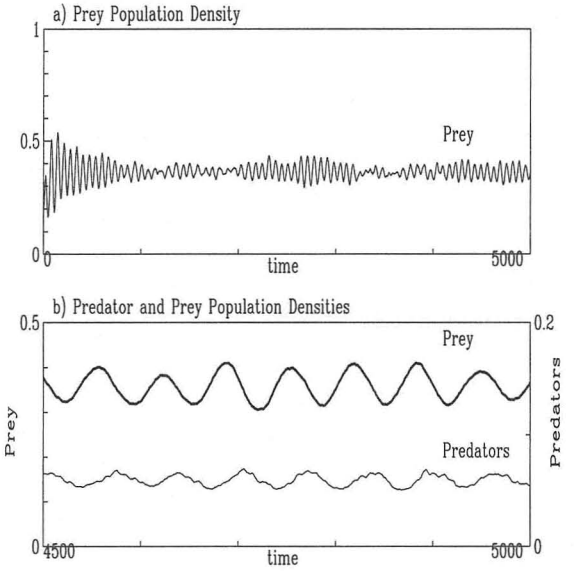

Figure 5: a) The prey population density from the initial random state at time $t = 0$ to $t = 5000$ for a simulation with the standard parameter set on a grid with $N = 300$. b) A close-up of the prey and predator population densities shown between times $t = 4500$ and 5000. The predator population lags the prey population. Superposed on the slow variations of the predator population cycle are fast variations which are related to the breeding time $sb = 8$ of the predators.

approximately constant period but with varying amplitude. Figure 5a shows the prey population from the initial random state to $t = 5000$ in a simulation with the standard parameter set on a grid with $N = 300$; over this time the population oscillates more than 70 times. A closer examination of the prey population between $t = 4500$ and $t = 5000$ in Figure 5b shows that the oscillations are regular though the amplitude may vary by as much as twenty percent of the average population, even after long times. The predator population, which is compared with the prey population in the lower diagram, has the same period as the prey population but lags in phase. Superposed on the predator population cycle is a fast variation, the period of which is a multiple of the predator breeding rate, $sb = 4$. The fast variation occurs because predators near a large cluster are unlikely to starve and these tend to have a single ancestor in common so that they breed at approximately the same time. The amplitude of the fast variation is large for small values of σ in equation (2) and for $\sigma < 0.1$ sympathetic fast variations are also observed in the prey population. For $\sigma = 0.5$, which we use for the simulations examined in detail here, the amplitude of the fast variations superposed on the prey population cycle is negligibly small.

Studies have been carried out about the dependence of the average predator and prey population on the parameters *fb*, *sb*, *ss*, and on the linear system size N. The populations of both species have been averaged over times between $t = 1000$ and $t = 10000$ for simulations with the standard parameters set on grids with $N = 50$, 100, 200, 300, and 400. The average population densities of the prey $\overline{P}_f$ and predators $\overline{P}_s$ are listed in Table 1. For $N > 100$, the average population of both predator and prey varies approximately as the area of the domain. That is, the average population density is independent of N for sufficiently large domains. For grids smaller than $N = 50$, boundary effects become significant as the natural cut-off cluster size is comparable to the domain size. For a variety of fixed parameter sets, we have performed 10 independent simulations on a grid with $N = 300$. The initial population densities of each species in the simulations are the same in each of the 10 cases, though the random initial placements of both species vary from case to case. The averages of $\overline{P}_f$ and $\overline{P}_s$ over the 10 cases are given in Table 1. For a wide range of parameters, the average population densities calculated in simulations on a smaller grid with $N = 100$ have been found to correspond within two percent of the average population densities calculated for the simulations with $N = 300$.

From Table 1 it is apparent that the average prey population density $\overline{P_f}$ increases as a function of decreasing predator starvation time *ss* and increasing predator breeding time *sb*. $\overline{P_f}$ is relatively insensitive to the breeding time *fb* of the prey. The average predator population density $\overline{P_s}$ increases with decreasing prey breeding time and is relatively insensitive to the predator breeding and starvation times. These trends agree, at least qualitatively, with those of the equilibrium populations predicted by the Lotka-Volterra equations (1): $(P_f, P_s) = (\alpha_s/\beta_2, \alpha_f/\beta_1)$. Here the death rate of predators in the absence of prey α_s is related to the inverse of the predator starvation time *ss* and the birth rate of prey α_f is related to the inverse of the prey breeding time *fb*. A more quantitative connection between the model results and the Lotka-Volterra equations (1) does not appear possible both because the dependence of the prey population on the predator birth rate does not appear explicitly in the equations and because the coefficients β_1 and β_2, which parametrize the effect of interactions between *homogeneously mixed* populations, may be not be defined explicitly in terms of the model parameters. Furthermore, unlike the Lotka-Volterra model, prey births occur only on the perimeter of clusters in our model, and so the growth rate is not proportional to the population in the absence of predators.

3.2 Age distribution of prey

Prey in the interior of clusters cannot breed and may therefore be much older than the breeding time *fb*. The distribution $D_N(A)$ of prey of age A is exponential for large A so that $D_N(A) \propto 2^{-A/A_0}$. Such a distribution is anticipated since the probability for prey either to be eaten or to give birth after they have been within a cluster for some time should not be a function of the

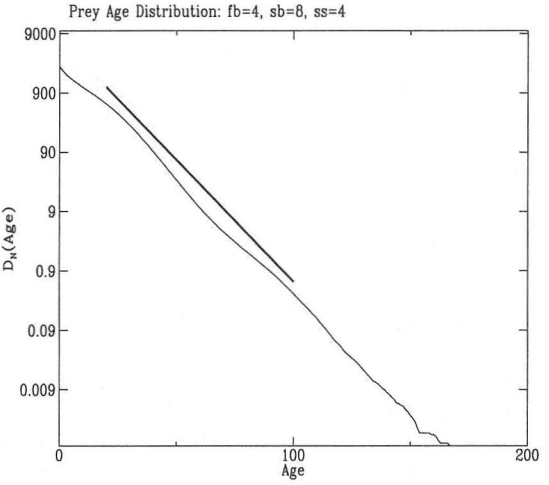

Figure 6: The prey age distribution calculated for times between $t = 1000$ and 10000 for a simulation with the standard parameter set on a grid with $N = 300$. For old prey, the distribution is close to exponential. The solid line represents the least-squares fit line to a log-plot of the distribution for ages between 20 and 100; the line is shifted above the distribution curve for clarity. Note that younger prey have a moderately smaller half-life than older prey.

age of the prey. Figure 6 shows the age distribution of prey calculated from a simulation over times between $t = 1000$ and 10000 for the standard parameter set on a grid with $N = 300$. The least-squares fit line to $\ln[D_N(A)]$ is calculated for $20 \leq A \leq 100$ and is shown in the figure shifted vertically above the distribution curve. Though there is some deviation from straight-line behavior for small A, the diagram shows that the age distribution of the older prey is approximately exponential and that this behavior persists for $A > 100$. The half-life of the older prey, which is determined from the slope of the least-squares fit line, is $A_0 \simeq 7.3$. The half-life of younger prey is marginally smaller (between 5 and 7) because breeding cannot take place within clusters and new-born prey are therefore more prone to be eaten or to give birth.

The half-life A_0 has been calculated for various parameter sets. These values, which are listed in Table 1, depend strongly on the prey breeding time but weakly on the predator breeding and starvation times. In other words, the prey half-life is a strong function of the parameter determining the prey source rate but is a weak function of the parameters determining the prey sink rate. Such behavior is readily understood because the dynamics governing the extraction of prey by predators do not depend on the age of prey that are long-lived and because the dynamics determining the source of prey explicitly requires new-born prey to have age zero.

3.3 Cluster distribution analysis

The prey positions at long times (e.g., Figures 2, 3, and 4) reveal that the prey organize into clusters of varying sizes and that there exists a natural cut-off size which is not due to the domain size. In this section we quantify these ideas.

A prey cluster is defined recursively as follows. A prey f_2 is said to belong to the same cluster as a prey f_1 either if f_2 is adjacent to f_1 (i.e., f_2 is situated at one of the four nearest neighbor positions of f_1) or if f_2 is adjacent to another prey f_3 which is also in the same cluster as f_1. The cluster size s is defined to be the number of prey in the cluster.

The cluster distribution function $D(s;t)$ is the number of clusters that have size s at time t. Analysis of the distribution function requires the calculation of the average $\overline{D}(s) = (1/n)\sum_{t=T_1}^{T_n} D(s;t)$ for large n (to improve the statistics) and sufficiently large T_1 (to remove the effect of the starting conditions). Small clusters are common, large clusters rare, and $\overline{D}(s)$ decreases with s. Because very large clusters (i.e., $s > 500$) occur with extremely low frequency, the distribution $\overline{D}(s)$ is noisy unless n is unreasonably large (i.e., $n > 10^6$), making analysis difficult. We have therefore used a binning procedure in which the binned distribution of the number of clusters of size s is the weighted average of the number of clusters with sizes in the neighborhood of s. We employ a Γ-distribution as a weighting factor since it is asymmetric about its mean and, for fixed a and b, $\Gamma(s;a,b)$ has a long tail for large s, thus giving more weight to sizes moderately smaller than s. The binned distribution function $D_\Gamma(s)$ is defined by

$$D_\Gamma(s) = \int_{s-1/2}^{s+1/2} d\tilde{s} \sum_{s'=1}^{\infty} \overline{D}(s')\Gamma(\tilde{s}; a(s'), b(s')) \tag{3}$$

in which a and b are set so that the mean and standard deviation of the Γ function are $ab = s'$ and $b\sqrt{a} = v(s')$, respectively. The standard deviation $v(s)$ is generally set to increase with larger s so that averages are taken over a wider range where data are sparse. Specifically, we set

$$v(s) = v_s(s-1) + v_0 \tag{4}$$

in which $v_s = 0.2$ and $v_0 = 0.1$. The results of the binning procedure are relatively insensitive to the values of v_s and v_0.

Figure 7 shows log-log plots of the unbinned and binned cluster distribution functions obtained using the standard parameter set on a grid with $N = 300$. The data are averaged over times between $t = 1000$ and 10000. The cluster distribution functions exhibit scaling behavior $D(s) \propto s^{-\alpha}$ over two ranges of cluster sizes, $1 < s < 20$ and $100 < s < 500$. Also shown on both diagrams are the least-squares fit lines to log-log plots of the data, calculated and plotted over the two ranges, shifted vertically above the data. The scaling exponents α' and α for small and large clusters are the slopes of the lines calculated for $1 \le s \le 20$ and $100 \le s \le 500$, respectively. For the unbinned distribution function shown in Figure 7a, $\alpha' = 2.35 \pm 0.07$ and $\alpha = 1.28 \pm 0.03$.

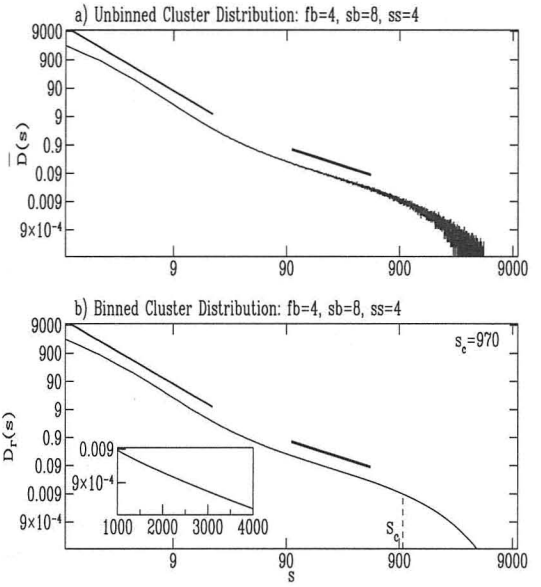

Figure 7: a) A log-log plot of the cluster distribution $\overline{D}(s)$ for the standard parameter set calculated on a grid with $N = 300$ for times between $t = 1000$ and 10000. The least-squares fit line with slope α' is found spanning the range $1 \leq s \leq 20$ and the least-squares fit line with slope α is found spanning the range $100 \leq s \leq 500$. Both lines are shifted above the distribution curve for clarity. b) The data in a) are binned to generate $D_\Gamma(s)$ shown in the bottom diagram. The least-squares fit lines calculated for this curve over the same two ranges have slope comparable to the corresponding lines for the raw data. The inset demonstrates the exponential behavior of the binned data for large s.

For comparison, the corresponding exponents calculated for the binned data shown in Figure 7b are $\alpha' = 2.34 \pm 0.07$ and $\alpha = 1.290 \pm 0.003$. The exponents calculated for the binned data are within the errors allowed by the least-squares fit to the unbinned data. The advantage of binning the data is clearly to reduce the magnitude of the error of the large-cluster exponent α by an order of magnitude and therefore enables better evaluation of the dependence of α on the parameters.

The least-squares fit lines to the binned data also provide a consistent definition of the cut-off scale s_c. For $s > s_c$, the number of clusters of size s decreases approximately exponentially as demonstrated by the inset to Figure 7b. We define s_c as the largest value of s for which the binned data lie within the error tolerances of the least-squares fit line to the unbinned data. That is, the cut-off size is set so that for $s > s_c$, $\ln[D_\Gamma(s)] < (-\alpha - \epsilon_\alpha)\ln(s) +$

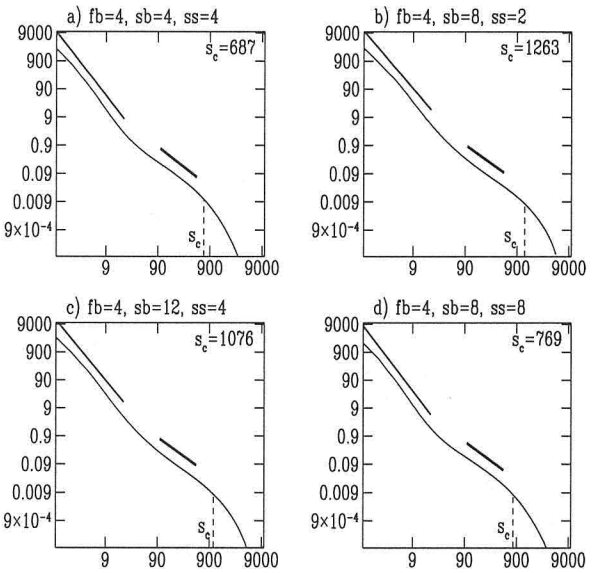

Figure 8: Log-log plots of the binned cluster distribution functions calculated for simulations on a grid with $N = 300$ for times between $t = 1000$ and 10000 with parameters a) $fb = 4$, $sb = 4$, $ss = 4$, b) $fb = 4$, $sb = 8$, $ss = 2$, c) $fb = 4$, $sb = 12$, $ss = 4$, and d) $fb = 4$, $sb = 8$, $ss = 8$. Least-squares fit lines calculated over ranges $1 \leq s \leq 20$ and $100 \leq s \leq 500$ in each diagram are shown shifted above the distribution function for clarity.

$(b_H - \epsilon_{b_H})$, in which $-\alpha$ and b_H are the slope and intercept, respectively, of the least-squares fit line to the unbinned data with ϵ_α and ϵ_{b_H} being the errors associated with the slope and intercept of this line. The cut-off size so calculated is shown in Figure 7b in which $s_c = 970$.

It is remarkable that the form of the cluster distribution function is relatively insensitive to the values of the breeding and starvation parameters. In Figure 8 the binned cluster distribution function is shown for the four parameter sets used to generate the clusters shown in Figure 4, but for simulations on grids with $N = 300$. The data are calculated for times between 1000 and 10000. The least-squares fit lines are shown over the ranges $1 \leq s \leq 20$ and $100 \leq s \leq 500$ and the cut-off size s_c is displayed in the upper right-hand corner of each diagram. All four cases shown are characterized by a steep scaling regime for small clusters and a regime with smaller scaling exponent for large clusters. The slopes calculated for the least-squares fit lines in both regimes vary little with the different parameter sets. In Table 1, the scaling exponents over both regimes are calculated by finding the mean of the exponents determined from 10 simulations with different initial conditions. In

all four cases, the small-cluster scaling exponent is approximately $\alpha' \simeq 2.3$ (± 0.1), although there is some tendency for this value to decrease with increasing predator breeding rate. Similarly, the large-cluster scaling exponent is $\alpha \simeq 1.35$ (± 0.10).

The different exponents for small and large clusters are believed to reflect the different predator-prey dynamics that occur when the prey form clusters large enough to have an interior. Large clusters are impervious to immediate attack and their growth is inhibited only when enough predators accumulate on the perimeter. Therefore larger clusters are longer lived. The small-cluster scaling breaks down for $s > 20$, which is of the correct size for a compact cluster with prey located entirely on the perimeter. Evidence for this assertion is provided by an analysis of simulations performed on three-dimensional grids; in such cases, log-log plots of the cluster distribution function (not shown here) exhibit a transitional range between small- and large-cluster scaling for $50 < s < 200$.

The cut-off cluster size s_c is determined by the time required for predators to find the prey and to multiply sufficiently to limit the expansion of large clusters. For a sufficiently large domain, the cut-off is not constrained by the domain size. The cut-off tends to be larger when the predator breeding time is significantly larger than both the prey breeding time and the predator starvation time. In this case the prey clusters accumulate to large sizes before the predators breed sufficiently to arrest their growth. The existence of the cut-off s_c means that the prey distribution function is subcritical. With increasing sb and decreasing ss, the cut-off increases so that the distribution becomes more critical and it appears that criticality can be approached arbitrarily closely in sufficiently large domains.

3.4 Radius of gyration of prey clusters

The distribution $\overline{D}(s)$ gives no information concerning the cluster geometry or, more specifically, it does not demonstrate how the linear extent of the prey clusters varies with size s. Therefore, we have examined the radius of gyration that for a particular cluster c_i is defined by

$$R(c_i) = \sqrt{\frac{1}{s_i} \sum_{j=1}^{s_i} |r_j|^2} \tag{5}$$

in which s_i is the size of c_i and r_j is the distance between the jth element of c_i and the center of mass of the cluster. The radius distribution function $R(s;t)$ is then defined to be the average radius of gyration of all clusters of size s at a time t. As with the definition of $\overline{D}(s)$, the mean radius distribution is defined by $\overline{R}(s) = (1/n) \sum_{t=T_1}^{T_n} R(s;t)$ for large n and sufficiently large T_1.

The sparsity of data for large cluster sizes results in variations of $R(s)$ which are too noisy for analysis. To smooth these data a harmonic mean

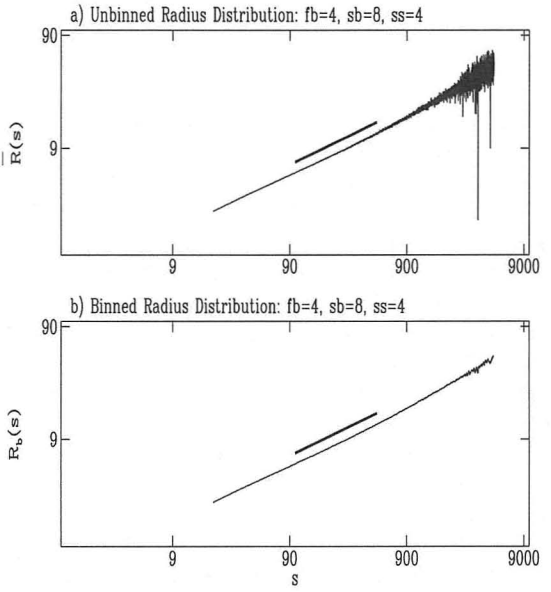

Figure 9: a) Log-log plot of the radius distribution $\overline{R}(s)$ calculated for a simulation with the standard parameter set on a grid with $N = 300$ for times between $t = 1000$ and 10000. The least-squares fit line with slope β is found spanning the range $100 \leq s \leq 500$. The line is shown shifted above the distribution for clarity. b) A harmonic mean binning procedure is applied to the data in a) to generate $R_b(s)$. Shifted above this curve is the corresponding least-squares fit line calculated over the same range as in a).

binning procedure is applied so that the binned radius distribution is

$$R_b(s) = \left[\prod_{s'=s-s_n}^{s+s_n} \overline{R}(s') \right]^{1/(2s_n+1)} \tag{6}$$

in which $s_n = \max(0, \lfloor 0.01(s-20) \rfloor)$ determines the bin size as an increasing function of s. (The notation $\lfloor x \rfloor$ denotes the largest integer not exceeding x.) Note that if this procedure is applied to a set of points sampled from a power-law distribution then the distribution is exactly recovered. If $\overline{R}(s)$, and hence $R_b(s)$, exhibits power-law behavior for large s so that $\overline{R} \propto s^\beta$, then the geometry of the clusters is characterized by the dimension $1/\beta$ which, if less than 2, is the fractal dimension [14].

Figure 9a shows the unbinned radius distribution calculated for times between $t = 1000$ and 10000 from a simulation with the standard parameter set on a grid with $N = 300$. The least-squares fit line to the data on a log-log plot is calculated for $100 \leq s \leq 500$ and provides a good fit over

this range with exponent $\beta = 0.505 \pm 0.006$. The exponent determined by a least-squares fit line to a log-log plot over the range $100 \leq s \leq 500$ of the binned data shown in Figure 9b is $\beta = 0.505 \pm 0.003$. In both cases the exponent is close to 0.5 as expected for a compact distribution (e.g., the size of the cluster varies as the square of the radius and so the clusters are objects of dimension 2). Indeed, for all the parameter sets we have examined on sufficiently large domains, the binned radius distribution function fits well to a 0.5 exponent for $100 \leq s \leq 500$. Prey clusters therefore exhibit weak, if any, fractal structure. We do note, however, that there appears to be some tendency toward lower dimensional scaling for large clusters ($s > 500$). This may be attributed to noise due to sparse data, or it may be that some lower dimensional structures develop when predators encompass a prey cluster with size $s > s_c$.

4. Conclusion

We have shown that Wa-Tor successfully simulates some basic features of predator-prey systems: the predator and prey populations vary quasi-periodically about respective average values and the predator population lags that of the prey; the average populations and the period of the oscillations are insensitive to the initial state; and the model is robust, in the sense that the system evolves nontrivially for a large range of parameters. In agreement with the predictions of the Lotka-Volterra equations, the average prey population density depends only on the breeding time and starvation times of predators, increasing with the former and decreasing with the latter. The average predator population density increases with increasing prey breeding time.

The prey naturally form clusters with a size distribution $\overline{D}(s)$ that varies as a power law over two ranges of s. For small clusters, the scaling exponent is $\alpha' = 2.3 \pm 0.1$ for a wide range of breeding and starvation parameters. The exponent tends to be smaller if the predator breeding time is large compared with either the starvation time or the prey breeding time. For large clusters $100 \leq s \leq 500$ the cluster distribution scales with a smaller exponent $\alpha = 1.35 \pm 0.10$. The exponent α tends to increase with increasing predator breeding time and decreasing prey breeding time, it is also large when the breeding time of predators and prey equal the starvation time of the predators. The scaling is appropriate for clusters of size smaller than a cut-off size $s_c \simeq 1000$.

We note that the model lies close to the edge of chaos, a state which Kauffman [12] has proposed may be optimal for adaptation. In the context of this model, the edge of chaos corresponds to power-law behavior (without a cut-off), the ordered state to a spanning cluster, and the chaotic state to small clusters only. Both the ordered and the chaotic states have limited biological viability. In the first, the population is in too strong contact; diversity and ultimately speciation are inhibited, and the species is too sensitive to disease. In the second, the population is too scattered to retain identity. It

is intriguing that a model with such simple rules has the desirable biological feature of lying close to the edge of chaos. The existence of a cut-off means that the system is subcritical; that is, it lies toward the chaos side of the edge of chaos, whereas Kauffman makes the hypothesis "Living systems exist in the solid regime near the edge of chaos...," (solid here meaning ordered). Subcriticality seems a desirable feature, since true power-law behavior would imply strong prey contact, inhibiting speciation.

Acknowledgments

This research was supported by the Natural Sciences and Engineering Research Council of Canada. We are grateful to Donn J. Kushner for references to the biological literature and to P. Bak and C. L. Henley for discussions and correspondence.

References

[1] P. Bak, K. Chen, and M. Creutz, "Self-organized Criticality in the Game of Life," *Nature*, **342** (1989) 780–782.

[2] P. Bak, C. Tang, and K. Wiesenfeld, "Self-organized Criticality," *Physical Review A*, **38(1)** (1988) 364–374.

[3] There are actually many Forest-Fire Models, some critical and some not. The original model appears not to be critical, but it displays highly interesting dynamics nonetheless, and has spawned a large literature. The following is an incomplete list of references: P. Bak, K. Chen, and C. Tang, *Phys. Lett.* A **147** (1990) 297–300; K. Chen, P. Bak, and M. H. Jensen, *Phys. Lett.* A **149** (1990) 207–210; P. Grassberger and H. Kantz, *J. Stat. Phys.* **63** (1991) 685–700; B. Drossel and F. Schwabl, *Phys. Rev. Lett.* **69** (1992) 1629–1632; W. K. Mosner, B. Drossel and F. Schwabl, *Physica* A **190** (1992) 205–217; P. Grassberger, *J. Phys. A: Math. Gen.* **26** (1993) 2081–2089; J. E. S. Socolar, G. Grinstein and C. Jayaprakash, *Phys. Rev.* E **47** (1993) 2366–2376; K. Christensen, H. Flyvbjerg and Z. Olami, *Phys. Rev. Lett.* **71** (1993) 2737–2740; C. L. Henley, *Phys. Rev. Lett.* **71** (1993) 2741–2744.

[4] D. Dab, A. Lawniczak, J.-P. Boon, and R. Kapral, "Cellular-automaton Model for Reactive Systems," *Physical Review Letters*, **64(20)** (1990) 2462–2465.

[5] A. K. Dewdney, *The Armchair Universe: An Exploration of Computer Worlds* (W. H. Freeman and Company, New York, 1988).

[6] A. Hastings, "Spatial Heterogeneity and Ecological Models," *Ecology*, **71** (1990) 426–428.

[7] L. R. Haury, J. A. McGowan, and P. H. Wiebe, "Patterns and Processes in the Time-space Scales of Plankton Distributions," in J. H. Steele, editor, *Spatial Pattern in Plankton Communities*, volume 3, (Plenum Press, New York, 1978).

[8] P. W. Hedrick, *Population Biology* (Jones and Bartlett Publishers, Inc., Boston, 1984).

[9] C. S. Holling, "Cross-scale Morphology, Geometry, and Dynamics of Ecosystems," *Ecological Monographs*, **62(4)** (1992) 447–502.

[10] T. Hwa and M. Kardar, "Dissipative Transport in Open Systems: An Investigation of Self-organized Criticality," *Physical Review Letters*, **62(16)** (1989) 1813–1816.

[11] L. P. Kadanoff, S. R. Nagel, L. Wu, and S. Zhou, "Scaling and Universality in Avalanches," *Physical Review A*, **39(12)** (1989) 6524–6537.

[12] S. A. Kauffman, *The Origins of Order* (Oxford University Press, New York, 1993).

[13] S. A. Levin, "Random Walk Models of Movement and their Implications," in T. G. Hallam and S. A. Levin, editors, *Mathematical Ecology* (Springer-Verlag Berlin, Heidelberg, 1986).

[14] B. B. Mandelbrot, *The Fractal Geometry of Nature* (W. H. Freeman, San Francisco, 1982).

[15] Y. Pomeau, "Invariant in Cellular Automata," *J. Phys. A*, **17** (1984) L415–L418.

[16] G. A. Rose and W. C. Leggett, "The Importance of Scale to Predator-prey Spatial Correlations: An Example of Atlantic Fishes," *Ecology*, **71** (1990) 33–43.